Int J Earth Sci (Geol Rundsch) (2007) 96:861–873
DOI 10.1007/s00531-006-0138-y

ORIGINAL PAPER

Variscan amphibolite-facies rocks from the Kurtoğlu metamorphic complex (Gümüşhane area, Eastern Pontides, Turkey)

Gültekin Topuz · Rainer Altherr · Winfried H. Schwarz · Abdurrahman Dokuz · Hans-Peter Meyer

Received: 1 September 2005 / Accepted: 19 September 2006 / Published online: 30 November 2006

Abstract The Kurtoğlu metamorphic complex, that forms part of the pre-Liassic basement of the Sakarya zone in northern Turkey, consists of at least two tectonic units. Blueschist-facies rocks of unknown metamorphic age in the southern part of the complex are tectonically overlain by Variscan low-pressure high-temperature metamorphic rocks. The latter comprise mica schists and fine-grained gneisses, cut by metaleucogranitic dikes, as well as migmatitic biotite gneisses and subordinate amphibolite intercalations. Structural data indicate that metamorphism and penetrative deformation occurred after dyke intrusion. Peak metamorphic conditions of the mica schists, fine-grained gneisses and metaleucogranites are estimated to ~650°C and ~0.4 GPa, based on phase relationships in the system NCKFMASH, Fe–Mg partitioning between garnet and biotite as well as garnet-aluminosilicate-quartz-plagioclase (GASP) and garnet-plagioclase-biotite-quartz (GBPQ) barometry. Peak temperatures of the migmatitic biotite gneisses and amphibolite intercalations are not well constrained but might have been significantly higher (690–740°C), as suggested from hornblende-plagioclase thermometry. ^{40}Ar–^{39}Ar incremental dating on muscovite and biotite fractions from the mica schists and fine-grained gneisses yielded plateau ages of ~323 Ma. Significantly older model ages of ~329 and ~337 Ma were obtained on muscovite fractions from two metaleucogranite samples. These fractions contain both relict igneous and newly formed metamorphic muscovite.

G. Topuz (✉)
Avrasya Yerbilimleri Enstitüsü,
Istanbul Teknik Üniversitesi,
TR-34469 Ayazağa, Istanbul, Turkey
e-mail: topuzg@itu.edu.tr

R. Altherr · W. H. Schwarz · H.-P. Meyer
Mineralogisches Institut, Universität Heidelberg,
Im Neuenheimer Feld 236, 69120 Heidelberg, Germany

A. Dokuz
Gümüşhane Mühendislik Fakültesi,
Jeoloji Mühendisliği Bölümü,
Karadeniz Teknik Üniversitesi,
TR-29000 Gümüşhane, Turkey

Introduction

The Sakarya zone in northern Turkey forms a ~1400 km long composite terrane, traceable from the Aegean coast of NW Turkey to the Lesser Caucasus in the east (Fig. 1). It consists of Jurassic and younger sedimentary and volcanic rocks that unconformably overlie a heterogeneous basement. This basement is still poorly known. To date, four different types of tectonic basement units have been identified: (1) A Variscan H*T*-L*P* metamorphic unit including gneisses, migmatites, amphibolites, marbles and ultramafic rocks (Okay 1996; Topuz et al. 2004a; Topuz and Altherr 2004); (2) Permocarboniferous molassic sediments (Okay and Leven 1996; Okay and Şahintürk 1997; Okay et al. 1997; Çapkınoğlu 2003); (3) low- to medium-grade metamorphic sequences of unknown age, intruded by late Carboniferous to early Permian granites (Çoğulu et al. 1965; Çoğulu and Krummenacher 1967; Delaloye et al. 1972; Delaloye and Bingöl 2000), and (4) strongly deformed and variably metamorphosed accretionary complexes comprising Permian to early Jurassic sedimentary and volcanic

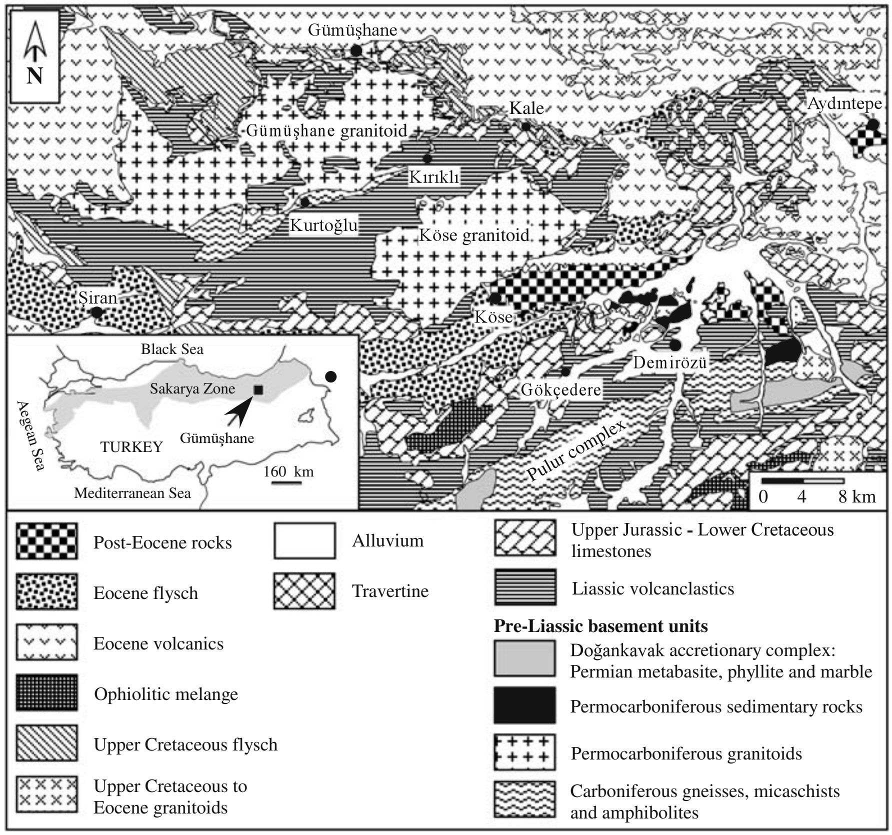

Fig. 1 Geological map of the Gümüşhane area as part of the Sakarya Zone in northern Turkey (inset)

sequences with exotic limestone blocks, attributed to the consumption of Palaeotethys (e.g. Okay and Göncüoğlu 2004; Topuz et al. 2004b; Yılmaz and Yılmaz 2004).

Deciphering the pre-Jurassic relationships between the various basement units of the Sakarya Zone is hampered by a lack of petrological and geochronological data. It is assumed that most of the basement of the Sakarya Zone was part of the southern margin of Eurasia in the latest Carboniferous, at the end of the Variscan orogeny (e.g. Stampfli and Borel 2002; Stampfli et al. 2002; Torsvik and Cocks 2004). In this paper, we present new and so far unique petrological and geochronological data on a medium-grade metamorphic sequence intruded by a late Carboniferous pluton (see type 3 above). This sequence forms part of the Kurtoğlu metamorphic complex, which is located near Gümüşhane in the eastern part of the Sakarya Zone (Fig. 1).

Geological setting

The Kurtoğlu metamorphic complex forms an elongated, ENE-WSW trending, ~26 km long and up to ~5 km wide exposure of metamorphic rocks along the southern boundary of the Gümüşhane I-type pluton (Fig. 2). This ~295 Ma old pluton covers an area of ~400 km^2 and consists of granite, granodiorite and quartz monzodiorite (Yılmaz 1974a–c, 1975; Çoğulu 1975; Topuz et al., unpublished data). At the contact with the Kurtoğlu metamorphic complex the plutonic rocks are fine-grained, suggesting a rather shallow intrusion depth. In contrast to the description of Yılmaz (1977), no obvious contact metamorphic overprint is observed in the metamorphic rocks. Locally, both the metamorpic complex and the Gümüşhane pluton are transgressively overlain by the Kelkit formation, a Liassic volcano-sedimentary series with a basal conglomerate.

To the south, the metamorphic rocks are bound by an ESE vergent thrust fault of post-Liassic age. At the southwestern end of the Kurtoğlu metamorphic complex, an undated microdioritic to gabbroic stock, crosscutting all the neighbouring lithologies, is exposed over an area of ~12 km^2 (Fig. 2).

The Kurtoğlu metamorphic complex consists of two different tectonic units: (1) a blueschist-facies metamorphic unit at the base, comprising phyllites, serpentinites, ophicarbonates and blueschists (Topuz et al., unpubl. data), and (2) a H*T*-L*P* metamorphic unit (Fig. 2). The latter unit, the topic of this paper, consists of a series of mica schists that include metaleucogranitic dikes. Both rock types have a common

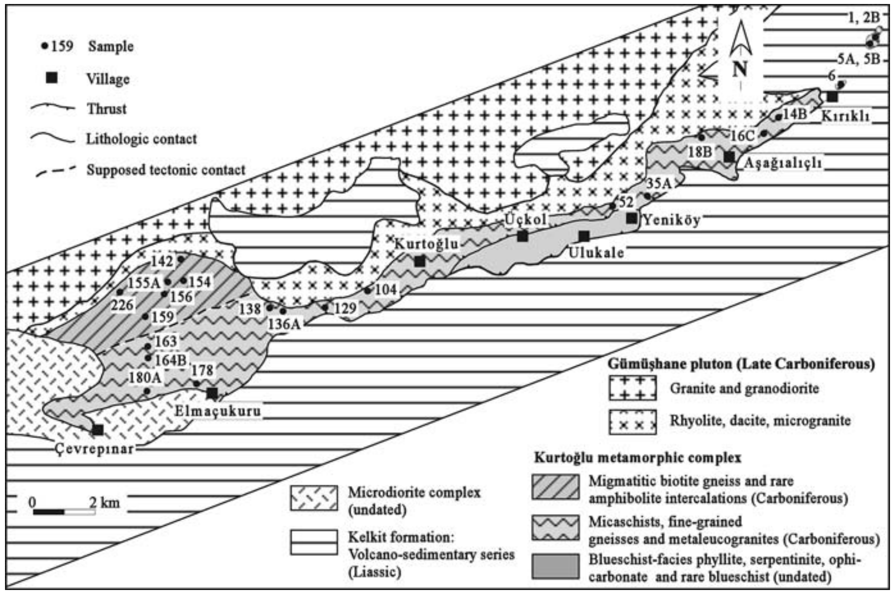

Fig. 2 Geological map of the Kurtoğlu metamorphic complex with sampling sites

foliation that is locally oblique to intrusive contacts, indicating that intrusion took place before metamorphism. In the southwestern part of the Kurtoğlu complex, migmatitic coarse-grained biotite gneisses with subordinate amphibolite intercalations occur to the north of the mica schists (Fig. 2).

Analytical techniques

Mineral analyses were carried out at the Mineralogisches Institut, Universität Heidelberg, using a Cameca SX 51 electron microprobe equipped five wavelength-dispersive spectrometers. Natural and synthetic oxide and silicate minerals were used for calibration. Standard operating conditions were 15 kV accelerationg voltage, 20 nA probe current and 10 s counting time for all elements except for Mg, Ca and Al (20 s) and Ti (30 s) in Fe–Ti oxides. Beam diameter was usually ~1 μm except for the analyses of feldspars (10 μm). Raw data were corrected for matrix effects with the help of the PAP algorithm (Pouchou and Pichoir 1984, 1985) implemented by Cameca. Detection limits were 0.03 wt% SiO_2, 0.06 wt% TiO_2, 0.06 wt% Al_2O_3, 0.07 wt% Cr_2O_3, 0.10 wt% FeO, 0.08 wt% MnO, 0.07 wt% MgO, 0.04 wt% CaO, 0.04 wt% Na_2O and 0.03 wt% K_2O.

$^{40}Ar/^{39}Ar$ incremental dating was performed at the Mineralogisches Institut, Universität Heidelberg. Large muscovite grains (>3 mm in diameter) from metaleucogranite samples were picked with tweezers under a binocular microscope, while biotite and muscovite fractions of finer grain sizes (125 – 315 μm) were obtained by conventional mineral separation techniques including cracking, sieving, magnetic and heavy liquid separation, hand picking and ultrasonic cleaning. Mineral fractions (ca. 15 mg) were wrapped into Al foil and several fractions were put into an evacuated and Cd-shielded quartz tube. Irradiation with $\sim 1.5 \times 10^{18}$ fast neutrons cm^{-2} was performed in the FRG-1 reactor of the Nuclear Research Center Geesthacht, Germany. Age and irradiation gradient monitoring was achieved by an in-house muscovite standard ('BMus', 326.2 ± 2.2 Ma, 2σ). Ar was extracted in a resistance-heated Ta furnace in a double-vacuum system up to 1,600°C. The blank level at 1,400°C was below the mass spectrometer detection limit of ca. 10^{-6} nl ^{40}Ar. First, H_2O and CO_2 from the extracted gas were frozen by using an acetone–CO_2 mixture. For further cleaning, Zr–Al getters were used. Ar isotope compositions were measured in a MAT GD-150 gas mass spectrometer (0.38 T permanent magnet, 180°, 5 cm radius of curvature) with no detectable argon background. Constants used for age calculations are those recommended by Steiger and Jäger (1977). $^{40}Ar/^{39}Ar$ age uncertainties comprise the errors of the $^{40}Ar/^{39}Ar$ ratios of irradiation monitors and age errors of the monitor. Measured $^{40}Ar/^{39}Ar$ data were corrected for irradiation interferences. All error assignments of isotope ratios and age given within this paper are within $\pm 1\sigma$.

Rock types and mineral compositions

Mica schists and fine-grained gneisses (MSG) from the H*T*-L*P* unit of the Kurtoğlu complex show a range of mineral assemblages and estimated abundances

(Table 1). Some rocks display compositional layering, whereby melanocratic layers rich in biotite and sillimanite alternate with leucocratic layers rich in either quartz or feldspar. In most samples, muscovite + quartz + plagioclase is a stable assemblage (Figs. 3a, b) and may be accompanied by either K-feldspar (samples 16C and 35A) or sillimanite (Fig. 3c). Sample 164A, however, contains K-feldspar including minor amounts of fibrolite, suggesting formation from muscovite + quartz. Muscovite textures do not suggest metastability. Two samples (14B, 180A) contain layers free of primary muscovite. In these samples, K-feldspar and sillimanite are clearly not in contact with each other, but occur in different layers. Either garnet or cordierite (totally pinitized) occur in some samples (Figs. 3d, e). Andalusite is present in two samples; in sample 138 it is intergrown with later sillimanite (Fig. 3f). In many samples, tourmaline is a minor or accessory phase. Graphite is generally absent.

Mineral compositions are nearly constant within individual samples but may vary significantly among samples. Muscovite is generally characterized by relatively low contents of Si (3.05–3.12 cpfu) and significant contents of Na (0.046–0.130 cpfu) (Table 2). Biotite has variable X_{Mg} [= Mg/(Mg+Fe_{tot})] ranging from 0.31 to 0.46 (Table 3); TiO_2 contents are relatively low (2.0–3.1 wt%). Garnet is rich in almandine and spessartine (Table 4 and Fig. 4). Plagioclase is Na-rich (An_{06}–An_{21}).

Metaleucogranitic dykes (MLG) consist of coarse-grained quartz, K-feldspar, albite, muscovite, ± tourmaline and accessory apatite and monazite. Porphyroclasts of K-feldspar ($Or_{95\text{-}92}Ab_{05\text{-}08}An_{00}$), albite ($Ab_{100\text{–}97}Or_{00\text{–}02}An_{00\text{–}01}$) and muscovite display strong intracrystalline deformational features such as grain scale faults, bent cleavage planes, deformation lamellae, patchy undulose extinction and subgrains with vague boundaries. Micrographic intergrowths of quartz and K-feldspar are widely preserved (Fig. 3g). A weak foliation is defined by fine-grained recrystallized muscovite intergrown with quartz and albite. Si contents in the cores of large relict igneous muscovite grains are generally low (3.05–3.11 cpfu), while recrystallized rims and small secondary grains are more Si-rich (3.12–3.27 cpfu), in particular in sample 18B (Table 2).

Migmatitic biotite gneisses (BG) are coarse-grained and consist of plagioclase, quartz, K-feldspar, biotite and accessory phases (Table 1). Textures are variable and range from stromatic via streaky to

Table 1 Mineral assemblages of mica schists, fine-grained gneisses and migmatitic biotite gneisses

Sample	Ms	Qtz	Pl	Kfs	Sil	And	Bt	Grt	Crd	Tur	Mnz	Apa	Zrn	Ilm
Mica schists and fine-grained gneisses (MSG)														
1	++	++	+	–	–	–	++	–	–	o	o	o	o	o
2B	++	++	+	–	+	–	++	+	–	o	o	o	o	–
5A	++	++	++	–	–	–	o	–	–	–	–	o	o	–
5B	++	++	+	–	+	–	++	+	–	o	o	o	o	–
14B layer 1	sec	+	+	–	++	–	++	–	+	–	o	o	o	–
14B layer 2	–	++	+	++	–	–	+	–	–	–	o	o	o	–
16C	+	++	+	+	–	–	++	–	–	–	–	o	o	–
35A	+	++	++	o	–	–	+	–	–	–	o	o	o	–
138 layer 1	++	++	++	–	+	+	++	–	–	+	o	o	o	–
138 layer 2	++	++	+	–	–	–	++	–	+	o	o	o	o	–
163	++	++	++	–	+	–	++	+	–	+	–	–	–	–
164A layer 1	+	++	++	o	–	–	o	–	–	o	o	o	o	o
164A layer 2	o	o	+	o	++	–	++	–	–	o	o	o	o	o
164B	++	++	++	–	–	+	–	–	–	+	–	–	–	–
180A layer 1	–	++	o	–	++	–	++	++	–	+	o	o	o	o
180A layer 2	+	+	++	+	–	–	+	+	–	o	o	o	o	–
180A layer 3	–	++	o	++	–	–	+	o	–	–	o	o	o	–
Migmatitic biotite gneisses (BG)														
142 melano	–	o	++	o	–	–	++	–	+	o	o	o	o	o
142 leuco	–	++	++	++	–	–	o	–	–	–	o	o	o	–
154	sec	++	++	+	–	–	+	–	o	o	o	o	o	–
155A	sec	++	++	++	–	–	+	–	–	o	o	o	o	–
159	–	++	++	++	–	–	+	–	o	o	o	o	o	–

++ major constituent; + minor constituent; o accessory phase; – not observed; sec secondary from plagioclase

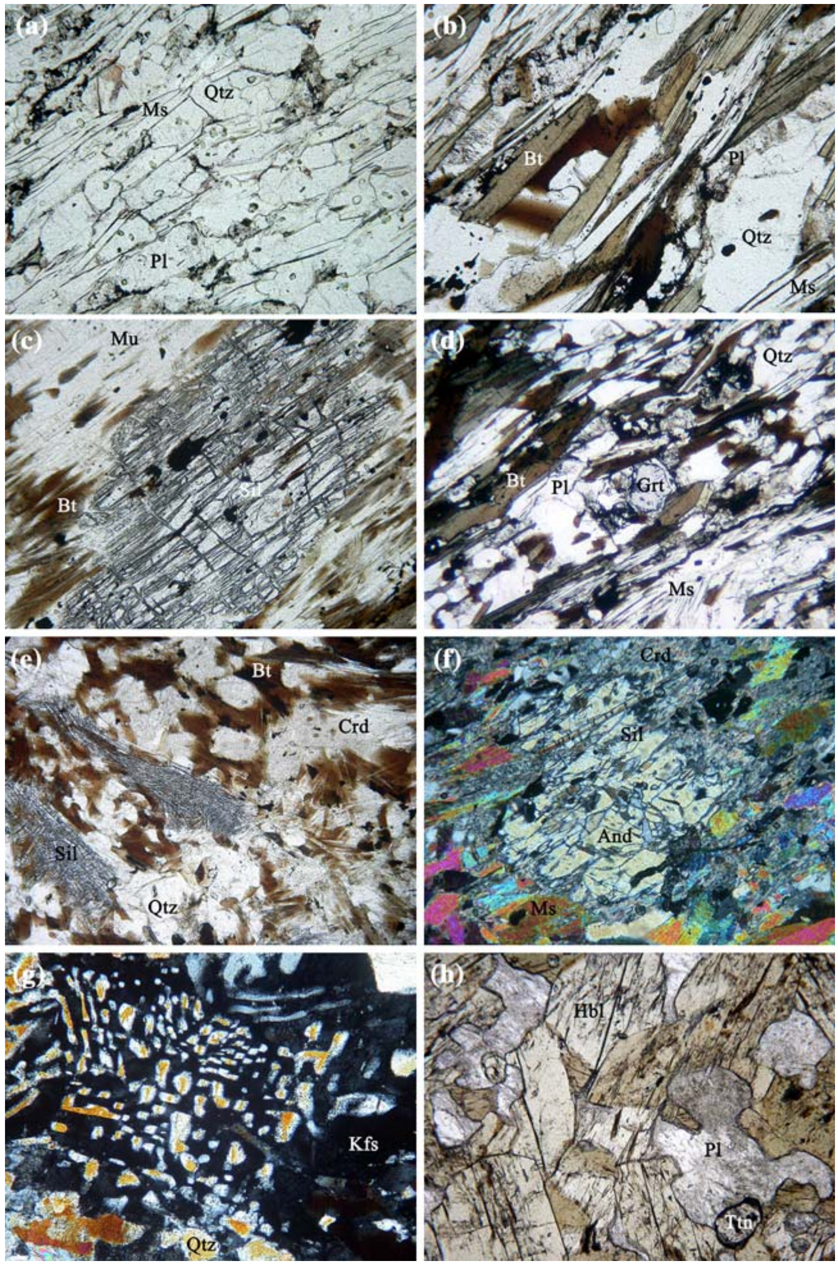

Fig. 3 Micrographs illustrating textural features of Kurtoğlu metamorphic rocks. (**a**) Muscovite schist with equilibrium assemblage Ms + Qtz + Pl (sample 5A). Muscovite defines the foliation and shares straight grain boundaries with quartz and plagioclase. (**b**) Muscovite-biotite schist with equilibrium assemblage Ms + Bt + Qtz + Pl (sample 1). (**c**) A thick sillimanite grain coexisting with biotite and muscovite (sample 5B). (**d**) Small garnet grain coexisting with Ms + Bt + Pl + Qtz (sample 5B). (**e**) Coexisting biotite + sillimanite + cordierite + quartz in layer 1 of mica schist sample 14B. (**f**) Aggregate of andalusite and later sillimanite in layer 1 of mica schist 138. (**g**) Relict micrographic intergrowths of Kfs and Qtz in a metaleucogranite (sample 27). (**h**) Coexisting hornblende, plagioclase and titanite in amphibolite (sample 227). In all micrographs, the width corresponds to 1.5 mm

homogeneous. Leucosomes are coarser than biotite-rich melanosomes and contain hypidiomorphic plagioclase. Biotite is characterized by higher TiO_2, compared to biotite from mica schists and fine-grained gneisses (Table 3). K-feldspar has the compositional range $Or_{80–97}Ab_{19–03}An_{01–00}$. Plagioclase is relatively calcic ($An_{27–42}$), whereby there is no systematic compositional difference between melanosomes and leucosomes.

Amphibolites are present in the form of up to 10 m thick intercalations within the biotite gneisses and consist of hornblende (Table 4) and plagioclase

Table 2 Selected representative electron microprobe analyses of muscovites from mica schists, fine-grained gneisses and metaleucogranites

Rock type	MSG	MSG	MSG	MSG	MSG	MSG	MSG	MSG	MSG	MSG	MLG	MLG	MLG	MLG	MLG	MLG	MLG	MLG
Sample no.	1	2B	5A	5B	16C	35A	138	163	164A	180A	18B	18B	29A	29A	104	104	136	136
Analysis no.	2	72	1	14	3	2	35	17	12	20	28	54	1	35	2	5	3	24
Type	met	met	met	met	met	met	met	met	met	met	ign	met	ign	met	ign	met	ign	met
SiO_2	47.86	46.67	46.79	46.20	46.08	46.00	46.52	46.59	47.47	45.88	45.82	48.85	46.74	47.35	46.85	47.85	46.61	47.72
TiO_2	0.60	0.53	0.49	0.86	0.48	0.89	0.31	0.72	0.72	0.17	0.32	0.29	0.20	0.26	0.38	0.10	0.06	0.04
Al_2O_3	36.10	35.97	35.23	36.03	35.70	34.50	36.96	36.89	36.17	36.43	36.00	30.68	36.63	35.72	36.62	35.36	35.63	34.53
Cr_2O_3	0.04	0.00	0.00	0.02	0.02	0.01	0.03	0.03	0.00	0.00	0.00	0.00	0.04	0.00	0.00	0.02	0.00	0.00
FeO	0.96	1.07	1.17	1.02	1.11	1.11	0.90	1.02	0.86	1.04	1.92	3.64	1.41	1.51	1.30	1.76	1.41	2.04
MnO	0.03	0.04	0.02	0.05	0.01	0.04	0.00	0.07	0.00	0.00	0.00	0.10	0.04	0.00	0.01	0.04	0.01	0.06
MgO	0.61	0.53	0.55	0.55	0.67	0.72	0.47	0.46	0.53	0.50	0.54	1.42	0.41	0.49	0.45	0.63	0.47	0.76
CaO	0.04	0.00	0.01	0.04	0.00	0.02	0.00	0.00	0.01	0.00	0.00	0.00	0.00	0.01	0.00	0.03	0.00	0.02
Na_2O	0.65	0.82	0.60	0.79	0.49	0.52	1.02	0.56	0.36	0.56	0.53	0.08	0.48	0.46	0.41	0.38	0.36	0.30
K_2O	9.23	9.64	9.80	9.44	10.27	10.26	9.52	9.03	10.03	9.82	9.82	9.89	9.69	9.86	9.96	9.57	10.31	10.14
Total	96.12	95.26	94.66	95.00	94.83	94.07	95.72	95.37	96.15	94.39	94.95	99.43	95.64	100.22	95.96	95.73	94.86	95.61
Si	3.119	3.086	3.114	3.062	3.072	3.096	3.057	3.061	3.104	3.062	3.059	3.274	3.077	3.119	3.076	3.146	3.105	3.158
Al(IV)	0.881	0.914	0.886	0.938	0.928	0.904	0.943	0.939	0.896	0.938	0.941	0.726	0.923	0.881	0.924	0.854	0.895	0.842
Al(VI)	1.892	1.889	1.878	1.877	1.877	1.833	1.919	1.918	1.891	1.927	1.891	1.698	1.920	1.892	1.910	1.885	1.903	1.851
Ti	0.030	0.026	0.024	0.043	0.024	0.045	0.015	0.036	0.036	0.008	0.016	0.015	0.010	0.013	0.019	0.005	0.003	0.002
Cr	0.002	0.000	0.000	0.001	0.001	0.000	0.002	0.001	0.000	0.000	0.000	0.000	0.002	0.000	0.000	0.001	0.000	0.000
Fe^{2+}	0.052	0.059	0.065	0.057	0.062	0.062	0.050	0.056	0.047	0.058	0.098	0.204	0.078	0.083	0.071	0.097	0.078	0.113
Mn	0.001	0.002	0.001	0.003	0.001	0.002	0.000	0.004	0.000	0.000	0.000	0.006	0.002	0.001	0.001	0.002	0.001	0.003
Mg	0.059	0.052	0.055	0.054	0.067	0.072	0.046	0.045	0.051	0.050	0.053	0.142	0.041	0.048	0.044	0.062	0.047	0.075
Ca	0.003	0.000	0.001	0.003	0.000	0.001	0.000	0.000	0.001	0.000	0.000	0.000	0.000	0.001	0.000	0.002	0.000	0.001
Na	0.082	0.105	0.078	0.101	0.064	0.067	0.130	0.071	0.046	0.072	0.068	0.011	0.062	0.059	0.052	0.049	0.046	0.038
K	0.768	0.813	0.832	0.798	0.874	0.881	0.798	0.757	0.836	0.836	0.836	0.845	0.814	0.829	0.834	0.803	0.876	0.856

Rock types: MSG, mica schists and fine-grained gneisses; MLG, metaleucogranite; Type: met, metamorphic; ign, relict igneous

Table 3 Selected electron microprobe analyses of biotite from mica schists, fine-grained gneisses and migmatitic biotite gneisses

Rock type	MSG	MSG	MSG	MSG	MSG	MSG	MSG	MSG	MSG	MSG	MSG	BG	BG
Sample no.	1	2B	5A	5B	14B	16C	35A	163	164A	180A	180A	142	154
Analysis no.	22	108	5	32	4	2	37	26	26	2	4	14	3
SiO_2	34.40	34.02	34.25	34.61	34.84	35.01	35.37	34.62	35.29	34.53	34.96	34.21	34.58
TiO_2	2.27	2.64	2.45	2.64	2.11	2.49	2.78	1.96	2.94	3.05	2.93	4.32	4.50
Al_2O_3	19.84	19.58	19.39	19.64	20.09	19.42	18.50	19.10	19.44	19.72	19.93	17.64	17.01
Cr_2O_3	0.01	0.05	0.02	0.03	0.06	0.06	0.07	0.09	0.04	0.03	0.06	0.06	0.02
FeO	21.94	21.00	23.67	20.57	19.54	18.98	19.52	22.43	18.46	20.72	18.93	22.48	22.39
MnO	0.28	0.42	0.33	0.36	0.32	0.42	0.26	0.16	0.21	0.52	0.64	0.28	0.24
MgO	7.19	7.34	5.94	8.29	8.09	8.79	8.73	7.28	8.85	7.22	8.53	7.56	7.41
CaO	0.00	0.01	0.00	0.00	0.04	0.00	0.00	0.01	0.00	0.00	0.00	0.00	0.00
Na_2O	0.28	0.22	0.18	0.29	0.17	0.14	0.17	0.23	0.13	0.22	0.20	0.20	0.19
K_2O	9.14	9.03	8.93	8.69	9.26	9.00	9.38	8.98	9.54	9.15	9.08	9.13	9.41
Total	95.35	94.31	95.24	95.12	94.53	94.31	94.77	95.85	94.89	95.15	95.27	95.88	95.75
Si	2.651	2.644	2.669	2.651	2.676	2.686	2.713	2.658	2.687	2.654	2.657	2.641	2.675
Ti	0.132	0.154	0.143	0.152	0.122	0.144	0.160	0.171	0.169	0.176	0.168	0.251	0.262
Al	1.802	1.794	1.777	1.773	1.819	1.756	1.672	1.729	1.745	1.787	1.785	1.605	1.551
Cr	0.001	0.003	0.001	0.002	0.004	0.003	0.004	0.005	0.002	0.002	0.003	0.004	0.001
Fe^{2+}	1.414	1.365	1.540	1.317	1.255	1.218	1.252	1.440	1.176	1.332	1.203	1.451	1.449
Mn	0.018	0.027	0.022	0.023	0.021	0.027	0.017	0.011	0.013	0.034	0.041	0.018	0.016
Mg	0.827	0.850	0.689	0.946	0.926	1.005	0.999	0.833	1.005	0.827	0.967	0.870	0.854
Ca	0.000	0.001	0.000	0.000	0.003	0.000	0.000	0.001	0.000	0.000	0.000	0.000	0.000
Na	0.042	0.033	0.028	0.044	0.026	0.021	0.025	0.033	0.018	0.033	0.030	0.030	0.029
K	0.898	0.895	0.886	0.849	0.907	0.881	0.918	0.880	0.927	0.897	0.880	0.899	0.928
X_{Mg}	0.369	0.384	0.309	0.418	0.424	0.450	0.444	0.366	0.461	0.380	0.450	0.372	0.371

Rock types: MSG, mica schist and fine-grained gneiss; BG, migmatitic biotite gneiss; X_{Mg} = Mg/(Mg + Fe)

Table 4 Selected electron microprobe analyses of garnet from mica schists and of hornblende from amphibolite

Mineral	Grt	Grt	Grt	Grt	Grt	Grt	Grt	Grt	Hbl	Hbl
Sample no.	2B	2B	5B	5B	163	163	180A	180A	226	226
Analysis no.	43	44	1	10	41	42	1	5	1	44
Domain	Core	Rim	Core	Rim	Rim	Core	Rim	Core	Rim	Core
SiO_2	36.30	36.47	36.37	36.34	36.58	36.58	36.75	36.68	49.73	48.83
TiO_2	0.00	0.00	0.00	0.01	0.02	0.00	0.00	0.02	1.13	1.64
Al_2O_3	21.15	21.09	20.63	20.94	20.50	20.60	20.62	20.81	6.17	7.13
Cr_2O_3	0.00	0.02	0.03	0.00	0.00	0.00	0.00	0.00	0.21	0.11
FeO_{tot}	31.34	30.81	30.73	30.27	31.30	31.51	27.55	28.96	11.42	11.76
MnO	9.16	9.52	9.16	9.87	9.92	9.56	12.90	11.50	0.29	0.24
MgO	1.91	1.76	1.96	1.78	1.97	2.36	1.78	2.06	15.23	14.68
CaO	0.60	0.86	0.61	0.46	0.41	0.38	0.60	0.69	11.39	12.03
Na_2O	0.01	0.00	0.00	0.01	0.03	0.00	0.02	0.02	0.86	0.96
K_2O	0.00	0.01	0.00	0.03	0.04	0.01	0.03	0.01	0.44	0.37
Total	100.47	100.54	99.49	99.71	100.78	100.99	100.25	100.73	96.87	97.73
Si	2.954	2.965	2.984	2.975	2.977	2.967	2.995	2.975	7.189	7.044
Ti	0.000	0.000	0.000	0.001	0.001	0.000	0.000	0.001	0.123	0.177
Al	2.028	2.021	1.994	2.021	1.966	1.969	1.980	1.989	1.051	1.051
Cr	0.000	0.001	0.002	0.000	0.000	0.000	0.000	0.000	0.024	0.012
Fe^{3+}	n.c.	n.c.	n.c.	n.c.	n.c.	n.c.	n.c.	n.c.	0.277	0.177
Fe^{2+}	2.133	2.094	2.109	2.073	2.130	2.137	1.878	1.964	1.104	1.241
Mn	0.631	0.655	0.636	0.684	0.684	0.657	0.890	0.790	0.036	0.029
Mg	0.231	0.213	0.239	0.217	0.239	0.285	0.216	0.249	3.282	3.156
Ca	0.053	0.075	0.053	0.040	0.036	0.033	0.053	0.060	1.765	1.859
Na	0.002	0.000	0.000	0.001	0.005	0.000	0.004	0.003	0.241	0.268
K	0.000	0.001	0.000	0.004	0.004	0.001	0.003	0.001	0.081	0.068
Total	8.032	8.025	8.017	8.016	8.043	8.049	8.018	8.031	15.173	15.082
X_{Alm}	0.70	0.69	0.69	0.69	0.69	0.69	0.62	0.64	–	–
X_{Pyp}	0.08	0.07	0.08	0.07	0.08	0.09	0.07	0.08	–	–
X_{Grs}	0.02	0.02	0.02	0.01	0.01	0.01	0.02	0.02	–	–
X_{Sps}	0.21	0.22	0.21	0.23	0.22	0.21	0.29	0.26	–	–

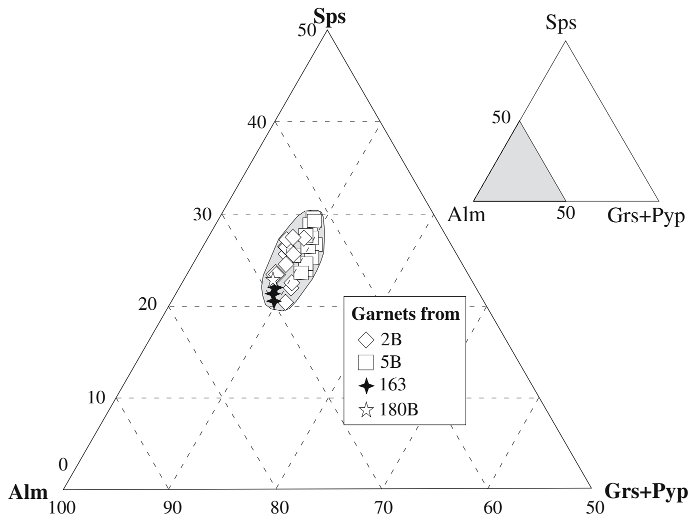

Fig. 4 Compositional variations of garnet in mica schists and fine-grained gneisses in terms of spessartine (Sps), almandine (Alm) and grossularite+pyrope (Grs + Pyp)

($An_{44–35}Ab_{54–60}Or_{\leq 02}$), accompanied by minor amounts of quartz, titanite and accessory apatite.

Metamorphic evolution

General considerations

Since the Kurtoğlu H*T*-L*P* metamorphic unit is exposed over a transect of ca. 26 km, peak *P*–*T* conditions recorded by the different samples may not necessarily overlap in a narrow field. Furthermore, the effects of variable bulk composition [e.g. X_{Mg} = Mg/(Mg + Fe), X_{Al} = Al/(Al + Mg + Fe)] and of water activity (aH_2O) on the location of multivariant reactions in the *P*–*T* space have to be considered. Our discussion of phase relationships and possible *P*–*T* conditions will be based on (1) phase relationships in the system $Na_2O–CaO–K_2O–FeO–MgO–Al_2O_3–SiO_2–H_2O$ (NCKFMASH), as outlined by White et al. (2001), and (2) thermobarometry.

Mica schists and fine-grained gneisses (MSG)

In samples 138 and 164B, andalusite is present. However, the additional presence of sillimanite in sample 138, and the coarse Ms at the border of resorbed And in sample 164B, suggest metastability of andalusite well within the Sil stability field. This hypothesis is in line with the interpretations of similar textures by other authors (e.g. Pattison 1992; Cesare et al. 2002).

Since all samples contain abundant OH-bearing phases, such as muscovite and/or biotite, and none of the samples contains graphite, we will assume a water activity (aH_2O) of unity, unless textures suggest the former presence of a melt phase. The assemblage Ms + Qtz + Pl + Bt + Sil (no Kfs) found in the NE (samples 2B, 5B) and SW (samples 138, 163 and 164B) of the Kurtoglu H*T*-L*P* unit (Fig. 2) is stable below ca. 630°C at 0.25 GPa and 725°C at 0.70 GPa for wide ranges of bulk X_{Mg} and X_{Al} (White et al. 2001). In the presence of H_2O, the solidus of this assemblage lies between ca. 655°C at 0.35 GPa and ca. 675°C at 0.60 GPa (White et al. 2001). Since rock textures do not suggest the former presence of melt in these samples (absence of leucosomes), peak temperatures should have been below the solidus (Fig. 6). The presence of garnet in samples 2B, 5B and 163 is most probably due to lower bulk X_{Mg}, compared with the other samples. This is in line with X_{Mg} values of biotite from these samples (Table 3).

In one sample (164A), textures suggest that Ms + Qtz + Pl + Sil + Kfs (+H_2O) was a stable assemblage. In the absence of melt, this assemblage is only stable within a small *P*–*T* field below the solidus (ca. 630–655°C and 0.28–0.36 GPa; NCKFMASH). The presence of significant amounts of Na in both Ms (Table 2) and Kfs indicates that this assemblage is at least divariant, implying that the peak metamorphic temperature of this sample was slightly below the univariant reaction curve Ms + Qtz = Sil + Kfs + H_2O in the KASH system.

Muscovite-bearing samples with assemblages devoid of Sil [e.g. Ms + Qtz + Pl + Bt ± (Kfs or Sil); Table 1 and Fig. 2] occur in close association with Sil-bearing samples, suggesting that the absence of Sil is due to lower bulk X_{Al} rather than different peak metamorphic conditions (see also White et al. 2001).

Two samples (14B, 180A) are characterized by the absence of stable Ms + Qtz. In these samples, Kfs and Sil are clearly not in contact to each other but occur in different layers, whereby Kfs forms part of the leucosomes (Qtz + Kfs + Pl + Bt), and Sil occurs in mesosomes and melanosomes, in coexistence with Bt + Grt or Crd ± Pl (Table 1). The general absence of primary Ms in sample 14B and its sparse occurrence in layer 2 of sample 180A (not in contact with quartz) in conjunction with the presence of leucosomes could be interpreted in terms of partial melting and breakdown of muscovite (in the presence of quartz). At high aH$_2$O and relatively low P (ca. 0.3 GPa), muscovite breakdown occurs prior to the solidus being crossed with increasing T. At 0.5 GPa, however, the solidus is at ca. 660°C, below the breakdown of muscovite at ca. 690°C (White et al. 2001). Hence, the fact that both, (Ms + Qtz)-bearing samples without leucosomes and samples without the stable assemblage Ms + Qtz but with leucosomes occur in close spatial association (compare Table 1 and Fig. 2), suggests that metamorphic peak conditions were generally near to the solidus in the NCKFMASH system, at pressures of ca. 0.4 GPa. Small differences in bulk composition, P, T and aH$_2$O may have been responsible for the fact that melting occurred in some samples but not in others.

In addition to the P–T constraints derived from phase relationships in the system NCKFMASH (Fig. 5), temperature estimates can also be obtained from Fe–Mg partitioning between garnet and biotite. Using the calibration of Ferry and Spear (1978), a wide range of temperature values between 517 and 631°C (at an assumed pressure of 0.4 GPa) is obtained for biotite-garnet contacts, whereby the values for small biotite inclusions in garnet tend to be lower than those for matrix biotite in contact with garnet. These temperature values should be regarded as closure temperatures for the Fe–Mg exchange between biotite and adjacent garnet. If the compositions of garnet rims (nearly identical with core compositions; Table 4) and biotite cores are used, temperature values between 615 and 660°C are obtained (Fig. 5). These values have to be regarded with some caution because of several effects, caused by the Mn-rich composition of garnets and the uncertainty of Fe^{3+} contents in biotite. It has been shown that for constant temperature, K_D [$K_D = (X_{Fe}/X_{Mg})^{Grt}/(X_{Fe}/X_{Mg})^{Bt}$] is negatively correlated with X_{Sps} in garnet. Therefore, temperature estimates derived from garnets with X_{Sps} 0.23 (Table 4), will be ca. 20–40°C lower than for a garnet with X_{Sps} 0 (Williams and Grambling 1990). On the other hand, biotite can contain significant amounts of Fe^{3+} and the $Fe^{3+}/\Sigma Fe$ ratio of biotite is quite variable and often higher than the value of 0.10, estimated for the experimental biotite used by Ferry and Spear (1978) for their calibration for which they assumed that all Fe in biotite was Fe^{2+} (see Williams and Grambling 1990 for discussion). Underestimation of $Fe^{3+}/\Sigma Fe$ in biotite will thus result in temperature estimates that are slightly

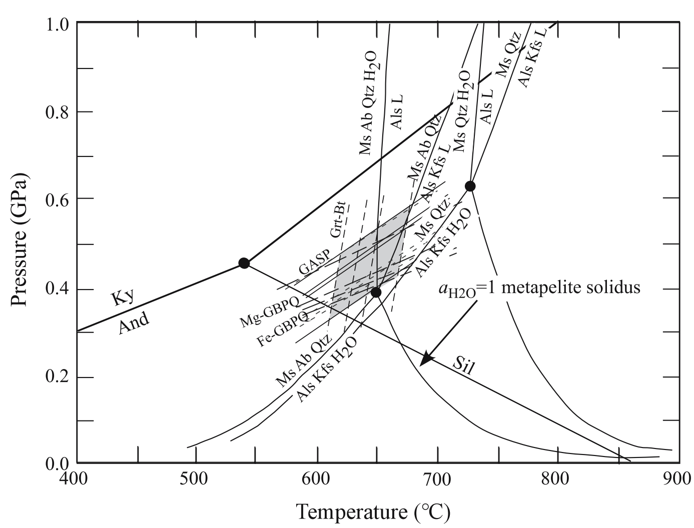

Fig. 5 *P*–*T* grid for NCKFMASH system after Spear et al. (1999). Steep dashed lines marked "Grt-Bt" are isopleths of Fe–Mg partitioning between biotite and garnet (core compositions) according to Ferry and Spear (1978). Thick solid lines are isopleths of GASP barometry (Koziol and Newton 1988; Koziol 1989). Thin solid lines and dashed lines are isopleths of GBPQ barometry for the Mg and Fe endmembers, respectively (Hoisch 1990, 1991). Grey area shows approximate equilibration conditions of Kurtoglu micaschists

too high. In combination, these two effects (Mn in garnet and Fe^{3+} in biotite) may nearly cancel.

For pressure estimates we used the garnet-aluminosilicate-quartz-plagioclase (GASP) barometer (Koziol and Newton 1988; Koziol 1989) and the garnet-plagioclase-biotite-quartz barometer (GBPQ) of Hoisch (1990, 1991). GASP isopleths for garnet and plagioclase rim compositions in the sillimanite-rich domains yielded pressures of 0.35–0.45 GPa at assumed temperatures of 600–650°C (Fig. 5). Pressure values obtained from the GBPQ barometer are nearly identical (Fig. 5). In addition, we used the garnet-rutile-ilmenite-aluminosilicate-quartz (GRAIL) barometer (Bohlen et al. 1983) to infer upper pressure limits for garnet core compositions (absence of rutile). Values for log K range from 0.38 to 0.42, resulting in a maximum pressure of 0.62 GPa at 650°C (Fig. 5).

Since the P–T estimates derived from geothermobarometry are nearly similar to those deduced from phase relationships in the system NCKFMASH, as outlined by White et al. (2001), we conclude that the schists and fine-grained gneisses were metamorphosed at peak conditions of ~650°C and ~0.4 GPa, whereby no systematic regional variation of peak metamorphic conditions was found (Fig. 5).

Migmatitic biotite gneisses and amphibolites

Metamorphic conditions for the migmatitic biotite gneisses are not well constrained. Both the existence of coarse-grained leucosomes and the presence of hypidiomorphic plagioclase grains indicate the former presence of a melt phase. As Crd is completely transformed to pinite, we do not know its former X_{Mg}; the X_{Mg} values of biotite are relatively low (Table 3), suggesting a 'normal' X_{Mg} of the bulk system. Hence, the presence of Crd and the general absence of Grt should indicate relatively low peak metamorphic pressures (<0.5 GPa; e.g. White et al. 2001).

Ad hoc, it is not possible to decide whether the inferred melt phase was formed by wet melting at low temperatures (ca. 680°C at 0.2 GPa and 650°C at 0.4 GPa) according to the reaction

$$\mathrm{Pl + Kfs + Qtz + H_2O = Liquid,}$$

or by dehydration melting at temperatures above ca. 730°C, according to the reaction

$$\mathrm{Bt + Sil + Pl + Qtz = Crd + Kfs + Liquid}$$

(Le Breton and Thompson 1988; Stevens et al. 1997). In the migmatitic biotite gneisses from Kurtoglu, the garnet-free assemblage Crd + Bt + Pl + Kfs (+Liq) is frequently observed. In the system NCKFMASH, this assemblage may be stable over a relatively large range of P–T conditions (i.e. up to ca. 780°C at 0.3 GPa, but not at pressures above ca. 0.45 GPa), depending on bulk composition (White et al. 2001).

Temperatures calculated from hornblende-plagioclase equilibria in amphibolite intercalations (Blundy and Holland 1990; Holland and Blundy 1994) range from 688 to 742°C at an assumed pressure of 0.4 GPa, whereby the pressure dependence is small. This temperature range is lower than the minimum temperatures needed for biotite dehydration melting to occur. On the other hand, this temperature range is significantly higher than that obtained for the mica schists and fine-grained gneisses, suggesting a fault between the migmatitic biotite gneisses and amphibolites in the north and the mica schists in the south (Fig. 2).

Age of metamorphism

^{40}Ar–^{39}Ar dating on two muscovite and one biotite separate from mica schists (samples 5A and 5B, same site) yielded plateau ages between 321.7 ± 1.9 and 324.3 ± 2.6 Ma (1σ; Table 5, Fig. 6), where the inte-

Table 5 Ar–Ar isotope data from muscovite and biotite fractions

Sample no. (mineral)	K (wt%)	$^{40}Ar^a$ (nl/g)	$^{40}Ar^a$ (%)	$^{40}Ar^a/^{39}Ar$	J value (10^{-4})	Total gas age (Ma)	Plateau age (Ma)
5A (Ms)	8.80	121.2 ± 1.0	97.77	34.66 ± 0.29	56.69 ± 0.17	323.6 ± 2.6 (2.8)	324.3 ± 2.6 (2.8)
5B (Ms)	8.38	113.6 ± 0.6	92.85	35.59 ± 0.22	54.31 ± 0.07	318.8 ± 1.8 (2.1)	321.7 ± 1.7 (2.1)
5B (Bt)	7.92	106.3 ± 0.6	90.65	35.48 ± 0.17	53.98 ± 0.20	316.1 ± 1.8 (2.1)	322.6 ± 1.9 (2.1)
104 (Ms)	9.87	138.1 ± 1.1	96.02	35.44 ± 0.20	56.29 ± 0.40	328.2 ± 2.7 (2.9)	328.2 ± 2.7 (2.9)
136A (Ms)	9.71	139.6 ± 0.8	97.51	36.71 ± 0.21	32.93 ± 0.04	336.6 ± 2.0 (2.3)	336.6 ± 2.0 (2.3)
154 (Bt)	6.31	79.3 ± 0.5	85.58	32.93 ± 0.20	54.41 ± 0.17	297.3 ± 1.8 (2.1)	320.3 ± 1.7 (2.1)*

K is estimated from the amount of ^{39}Ar. Errors given are ±1σ. Errors in parentheses comprise age error and uncertainty of standard. An in-house standard, 'Bmus' (Bärhalde muscovite), calibrated against MMHb1, was used; age, K content and $^{40}Ar^a$ content are 326.2 ± 1.1 Ma (1σ), 8.47 wt% and 117.7 nl/g, respectively

[a] Minimum age corresponding to the 11th step of the age spectrum due to loss of Ar (see text for explanation)

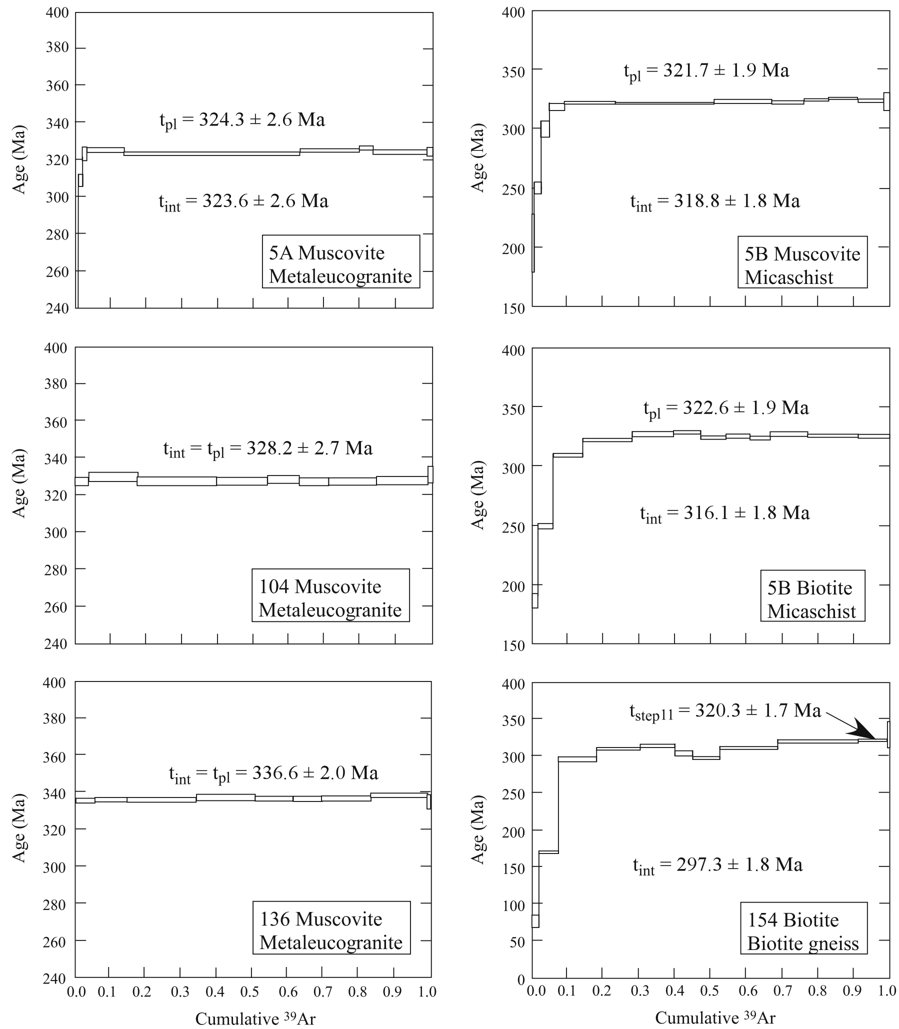

Fig. 6 ^{40}Ar–^{39}Ar release spectra of muscovite and biotite fractions from metamorphic rocks of the Kurtoğlu complex. See text (‘age of metamorphism’) for further explanation

grated age of 5A muscovite is indistinguishable from its plateau age and the integrated ages of 5B samples are slightly younger than the plateau age, especially for the biotite sample. Muscovite separates from two metaleucogranite samples yielded plateau ages of 328.2 ± 2.7 (sample 104) and 336.6 ± 2.0 Ma (sample 136) for the total release of the argon. From the biotite gneiss sample 154 an integrated age of 297.3 ± 1.8 Ma is obtained. There is a significant discrepancy in muscovite ages, in particular between samples 136 and 5A/B.

There are two different types of muscovite in the metaleucogranites (see chapter ‘Rock types and mineral compositions’): (1) coarse-grained (up to 1 mm) igneous muscovites and (2) fine-grained metamorphic muscovite, the latter being similar to muscovite from the micaschists and fine-grained gneisses. In sample 136, the muscovite separate contained only a very small amount of fine-grained metamorphic muscovite. So the plateau and integrated ages of 336.6 ± 2.0 Ma can be interpreted as the cooling age of the leucogranitic dikes, prior to the peak of metamorphism. In contrast, the muscovite separate from the second metaleucogranite sample (104) contains approximately equal amounts of both muscovite generations. This may explain the slightly elevated ages of this sample, as compared to the ages of samples 5A and 5B (Table 5).

Biotite from samples 5B and 154, and, to a lesser extent, muscovite from sample 5B, show some loss of radiogenic argon due to a hydrothermal overprint, documented by the formation of minor amounts of chlorite from biotite (at temperatures between 200 and 400°C). This loss of argon is suggested by the ‘staircase’-type age spectra (Fig. 6). In sample 5B, biotite is more affected than muscovite, possibly due its slightly lower ‘closure temperature’ (Villa 1998). Biotite from sample 154 (migmatitic biotite gneiss from the southwestern part of the complex) with an integrated age of 297.3 ± 1.8 Ma shows the largest loss of radiogenic argon. This aliquot contains a significant amount of chlorite (compare calculated K content from the data given in Table 5), although considerable efforts were made during separation. The whole Ar release spectrum is characterized by stairs, suggesting argon loss from the whole biotite grains. Therefore, the last (significant) step 11 with an age of 320.3 ± 1.7 Ma may only represent a minimum age for the metamorphic event. On the other hand, this minimum age is only slightly lower than the plateau age of biotite 5B (Table 5). The hump shape of both biotite spectra are an artefact of the ^{40}Ar–^{39}Ar method, produced by the recoil of argon from the biotite-chorite interlayering during irradiation (Di Vincenco et al. 2003). From the age spectra (that are flat over 85% of ^{39}Ar release) and additional isochron studies (not shown), there is no evidence for inherited or excess argon in all investigated samples.

The loss of argon from biotites 5B and 154 and from muscovite 5B may have been caused by the intrusion of the Gümüshane plutonic complex at c. 295 Ma (own unpublished data). Temperatures reached after the intrusion at sample locations 5B and 154 cannot be estimated but should be equal to or higher than the 'closure temperature' of biotite (ca. 450°C; Villa 1998) and lower or equal to that of muscovite (ca. 500°C; Villa 1998).

Discussion and conclusion

The Kurtoğlu schists, gneisses and amphibolites bear no evidence for a Mesozoic or Cenozoic rejuvenation as observed in other occurrences of Variscan basement in the Sakarya Zone, such as the Kazdağ and Uludağ complexes in NW Turkey (Okay and Satır 2000, oral communication 2005). Apart from the Variscan Cenci unit in the Pulur complex (Topuz et al. 2004a; Topuz and Altherr 2004), the Kurtoğlu metamorphic rocks represent the second well-defined example of Variscan basement that escaped Mesozoic and/or Cenozoic overprint related to the closures of Paleotethys and Neotethys, respectively.

The Variscan high-T low-P units in the Kurtoğlu and Pulur complexes display remarkable lithologic differences. In the Pulur complex, amphibolite and ultramafic rocks form a major constituent of the Cenci unit, while such rocks are rare in the Kurtoğlu complex. Furthermore, the occurrence of metaleucogranites is restricted to the Kurtoğlu complex. Compared with the low-T granulites from the Pulur complex that were subject to peak conditions of >800°C and 0.7–0.8 GPa, the mica schists, fine-grained gneisses and metaleucogranites from Kurtoğlu were metamorphosed at significantly lower temperatures of ~650°C and pressures of ~0.4 GPa. For the migmatitic biotite gneisses and amphibolites, temperatures might have been somewhat higher (~720°C).

Acknowledgments This paper benefited from constructive reviews of Bernardo Cesare and Sarah C. Sherlock as well as from fruitful discussions with Aral I. Okay, Yücel Yılmaz and Cüneyt Şen. Special thanks are due to Murat Kayıkçı for cutting rock slices and Ilona Fin and Oliver Wienand for preparing high-quality thin sections. Yener Eyüboğlu, Mutlu Sarıkaya and Özgür Parlak are thanked for their companionship during field work that was financially supported by grant # 104Y284 of the Scientific and Technological Research Council of Turkey (TÜBITAK).

References

Blundy JD, Holland TJB (1990) Calcic amphibole equilibria and a new amphibole-plagioclase geothermometer. Contrib Mineral Petrol 104:208–224

Bohlen SR, Wall VJ, Boettcher AL (1983) Experimental investigations and geological applications of equilibria in the system FeO–TiO_2–Al_2O_3–SiO_2–H_2O. Am Mineral 68:1049–1058

Çapkinoğlu S (2003) First records of conodonts from the Permo-Carboniferous of Demirözü (Bayburt), Eastern Pontides, NE Turkey. Turk J Earth Sci 12:199–217

Cesare B, Gómez-Pugnaire MT, Sánchez-Navas A, Groberty B (2002) Andalusite-sillimanite replacement (Mazarrón, SE Spain): a microstructural and TEM study. Am Mineral 87:433–444

Çoğulu E (1975) Gümüşhane ve Rize bölgelerinde petrolojik ve jeokronolojik araştırmalar. Istanbul Teknik Üniversitesi Yayını 1034:112

Çoğulu E, Krummenacher D (1967) Problèmes géochronométriques dans le partie NW de l'Anatolie Centrale (Turquie). Schweiz Mineral Petrogr Mitt 47:825–831

Çoğulu E, Delaloye M, Chessex R (1965) Sur l'âge de quelques roches plutoniques acides dans la région d'Eskişehir, Turquie. Archives des Sciences Genève 18:692–699

Delaloye M, Bingöl E (2000) Granitoids from western and northwestern Anatolia: Geochemistry and modeling of geodynamic evolution. Intern Geol Rev 42:241–268

Delaloye M, Çoğulu E, Chessex R (1972) Geochronometric study on crystalline massifs Rize and Gümüşhane. Compte Rendu des Séances de la Societé de Physique et D'Histoire Naturelle De Genève 7:43–52

Di Vincenco G, Viti C, Rocchi S (2003) The effect of chlorite interlayering on 40Ar–39Ar biotite dating: an 40Ar–39Ar laser-probe and TEM investigations of variably choritised biotites. Contrib Mineral Petrol 145:643–658

Ferry JM, Spear FS (1978) Experimental calibration of partitioning of Fe and Mg between biotite and garnet. Contrib Mineral Petrol 66:113–117

Hoisch TD (1990) Empirical calibration of six barometers for the mineral assemblage quartz+muscovite+biotite+plagioclase+garnet. Contrib Mineral Petrol 104:225–234

Hoisch TD (1991) Equilibria within the mineral assemblage quartz + muscovite + biotite + garnet + plagioclase, and its implications for the mixing properties of octahedrally

coordinated cations in muscovite and biotite. Contrib Mineral Petrol 108:43–54
Holland T, Blundy J (1994) Non-ideal interactions in calcic amphiboles and their bearing on amphibole-plagioclase thermometry. Contrib Mineral Petrol 116:433–447
Koziol AM (1989) Recalibration of the garnet-plagioclase-Al_2SiO_5-quartz (GASP) geobarometer and applications to natural parageneses. EOS Trans Am Geophys Union 70:493
Koziol AM, Newton RC (1988) Redetermination of anorthite breakdown reaction and improvement of the plagioclase-garnet-Al_2SiO_5-quartz geobarometer. Am Mineral 73:216–223
Le Breton N, Thompson AB (1988) Fluid-absent (dehydration) melting of biotite in metapelites in the early stages of crustal anatexis. Contrib Mineral Petrol 99:226–237
Okay AI (1996) Granulite facies gneisses from the Pulur Region, Eastern Pontides. Turk J Earth Sci 5:55–61
Okay AI, Leven E-J (1996) Stratigraphy and paleontology of the upper Paleozoic sequences in the Pulur (Bayburt) region, Eastern Pontides. Turk J Earth Sci 5:145–155
Okay AI, Şahintürk Ö (1997) Geology of the Eastern Pontides. In: Robinson AG (ed) Regional and petroleum geology of the Black Sea and surrounding region. Am Ass Petrol Geol (AAPG) Memoir 68, pp 291–311
Okay AI, Satır M (2000) Coeval plutonism and metamorphism in a latest Oligocene metamorphic core complex in northwest Turkey. Geol Mag 137:495–516
Okay AI, Göncüoğlu MC (2004) The Karakaya complex: a review of data and concepts. Turkish J Earth Sci 13:77–95
Okay AI, Şahintürk Ö, Yakar H (1997) Stratigraphy and tectonics of the Pulur (Bayburt) region in the eastern Pontides. Mineral Res Expl Bull 119:1–24
Pattison DRM (1992) Stability of andalusite and sillimanite and the Al_2SiO_5 triple point: Constraints from the Ballachulish aureole, Scotland. J Geol 100:423–446
Pouchou JL, Pichoir F (1984) A new model for quantitative analyses. I. Application to the analysis of homogeneous samples. La Recherche Aérospatiale 3:13–38
Pouchou JL, Pichoir F (1985) ‘‘PAP’’ (Φ–ρ–Z) correction procedure for improved quantitative microanalysis. In: Armstrong JT (ed) Microbeam analysis. San Francisco Press, USA, pp 104–106
Spear FS, Kohn MJ, Cheney JT (1999) P-T paths from anatectic pelites. Contrib Mineral Petrol 134:17–32
Stampfli GM, Borel GD (2002) A plate tectonic model for the Paleozoic and Mesozoic constrained by dynamic plate boundaries and restored synthetic oceanic isochrons. Earth Planet Sc Lett 196:17–33
Stampfli GM, von Raumer JF, Borel GD (2002) Paleozoic evolution of pre-Variscan terranes: from Gondwana to the Variscan collision. In: Martínez Catalán JR, Hatcher RD Jr, Arenas R, Díaz García F (eds) Variscan-Appalachian dynamics: The building of the late Paleozoic basement, Boulder Colorado, Geol Soc Am Spec Pap 364, pp 263–280
Steiger RH, Jäger E (1977) Subcommission on Geochronology: Convention on the use of decay constants in geo- and cosmochronology. Earth Planet Sci Lett 36:359–362
Stevens G, Clemens JD, Droop GTR (1997) Melt production during granulite-facies anatexis: experimental data from ‘‘primitive’’ metasedimentary protoliths. Contrib Mineral Petrol 128:352–370
Topuz G, Altherr R (2004) Pervasive rehydration of granulites during exhumation—an example from the Pulur complex, Eastern Pontides, Turkey. Mineralogy and Petrology 81:165–185
Topuz G, Altherr R, Kalt A, Satır M, Werner O, Schwarz WH (2004a) Aluminous granulites from the Pulur complex, NE Turkey: a case of partial melting, efficient melt extraction and crystallization. Lithos 72:183–207
Topuz G, Altherr R, Satır M, Schwarz WH (2004b) Low-grade metamorphic rocks from the Pulur complex, NE Turkey: implications for the pre-Liassic evolution of the Eastern Pontides. Int J Earth Sci 93:72–91
Torsvik TH, Cocks LRM (2004) Earth geography from 400 to 250 Ma: a palaeomagnetic, faunal and facies review. J Geol Soc London 161:555–572
Villa IM (1998) Isotopic closure. Terra Nova 10:42–47
White RW, Powell R, Holland TJB (2001) Calculation of partial melting equilibria in the system Na_2O–CaO–K_2O–FeO–MgO–Al_2O_3–SiO_2–H_2O (NCKFMASH). J Metam Geol 19:139–153
Williams ML, Grambling JA (1990) Manganese, ferric iron, and the equilibrium between garnet and biotite. Am Mineral 75:886–908
Yılmaz Y (1974a) Geology of the Gümüşhane granite (petrography). Istanbul Üniversitesi, Fen Fakültesi Mecmuası B39:157–172
Yılmaz Y (1974b) Geochemical study of the Gümüşhane granite. Istanbul Üniversitesi, Fen Fakültesi Mecmuası Seri B39:173–204
Yılmaz Y (1974c) History of the cyrstallization of the Gümüşhane granite. Istanbul Üniversitesi, Fen Fakültesi Mecmuası Seri B39:205–210
Yılmaz Y (1975) Emplacement of the Gümüşhane granite. Cumhuriyetin 50, Yılı Yerbilimleri Kongresi, Tebliğler, MTA Ankara, pp 485–489
Yılmaz Y (1977) Kurtoğlu dokanak metamorfizma kuşağinda bazı petrojenetik sorunlar. Türkiye Jeoloji Kurumu Bülteni 20:63–68
Yılmaz A, Yılmaz H (2004) Geology and Structural Evolution of the Tokat Massif (Eastern Pontides, Turkey). Turk J Earth Sci 13:231–246